International Journal of Fatigue 100 (2017) 148–158

Contents lists available at ScienceDirect

International Journal of Fatigue

journal homepage: www.elsevier.com/locate/ijfatigue

Microstructural changes in White Etching Cracks (WECs) and their relationship with those in Dark Etching Region (DER) and White Etching Bands (WEBs) due to Rolling Contact Fatigue (RCF)

Viktorija Šmeļova [a,b,*], Alexander Schwedt [b], Ling Wang [a], Walter Holweger [a,c], Joachim Mayer [b]

[a] National Centre for Advanced Tribology at Southampton (nCATS), University of Southampton, University Road, Southampton SO17 1BJ, UK
[b] Central Facility for Electron Microscopy (GFE), RWTH Aachen University, Ahornstraße 55, 52074 Aachen, Germany
[c] Schaeffler Technologies AG & Co. KG, Industriestraße 1-3, 91074 Herzogenaurach, Germany

ARTICLE INFO

Article history:
Received 14 December 2016
Received in revised form 18 March 2017
Accepted 22 March 2017
Available online 23 March 2017

Keywords:
Steel
Electron microscopy
White Etching Cracks (WECs)
White Etching Area (WEA)
Rolling Contact Fatigue (RCF)

ABSTRACT

Substantial microstructural changes, such as Dark Etching Region (DER), White Etching Bands (WEBs) and White Etching Cracks (WECs), can occur in typical bearing steels such as AISI 52100 and 4320 due to Rolling Contact Fatigue (RCF). Although it has been reported that DER and WEBs typically appear in bearings over extended rolling cycles (>100 × 10^6) as a result of material deterioration under high-stress RCF while WECs are found to occur in much earlier of bearing's life (<20% the calculated L_{10} life), differences and relationship between DER/WEBs and WECs are not fully investigated or understood. This study investigated the microstructural alterations in WECs in an AISI 52100 through-hardened martensitic bearing using a combination of characterisation methods and the results are directly compared with those observed in DER and WEBs due to high-stress RCF (Šmeļova et al., 2017). The results show that, although the features maybe initiated by different causes, there are many similarities between the microstructural alterations in WECs and DER/WEBs, such as the carbide disintegration, and carbon and chromium movement that plays a role in the formation and development of microstructural alterations in all three features.

1. Introduction

In recent years, ambitious worldwide renewable energy targets have resulted in significant growth of the wind energy sector's market share. Total installation of wind turbines in Europe has roughly increased by a factor of 10 since 2000 [2,3]. Size and capacity of wind turbines have also increased significantly, resulting in the use of larger multistage gearboxes. Statistics revealed that larger wind turbines experience higher failure rates compared to small turbines and gearbox bearings in large wind turbines have particular low overall reliability compared with other components [4–6]. The average wind turbine gearbox bearing life has been reported as early as a few years of service despite their 20 years of designed life [7–11]. Although bearings have been found to fail due to many reasons, such as inadequate lubrication, deficient sealing, improper mounting, overloading, or other tribological issues [12,13], White Structure Flaking (WSF) due to White Etching Cracks (WECs) has been reported to be one of the main failure modes in wind turbine gearbox bearings. WSF has also been reported in a wide range of different engineering applications, such as aircraft engine gears and bearings [14], paper mills [15,16], train rail tracks and wheels [17,18], marine propulsion systems [15], automotive alternators [15,16,19], water pumps [8], screw vacuum pumps [20], washing machines and others [21]. It has been commonly accepted that WSF due to WEC is different from the Rolling Contact Fatigue (RCF) failures because WECs occur much earlier (typically within 10–20% calculated bearing L_{10} life). Additionally, WECs do not always form along the directions of maximum shear stresses and appear to be random networks without preferred locations or direction of growth [11,22,23]. Majority WECs are subsurface microcrack networks that form within 1.5 mm below the contact surface [8,17]. They vary from several μm to mm in size and appear to be parallel or branching networks depending on the cross-section plane in a bearing being viewed. Compared with Dark Etching Region (DER) and White Etching Bands (WEBs) formed under medium to high stresses over hundreds million rolling cycles due to RCF, WECs have no obvious relation to the

* Corresponding author at: National Centre for Advanced Tribology at Southampton (nCATS), University of Southampton, University Road, Southampton SO17 1BJ, UK.
E-mail address: v.smelova@soton.ac.uk (V. Šmeļova).

http://dx.doi.org/10.1016/j.ijfatigue.2017.03.027
0142-1123/

apparent pressure [23,24]. In the circumferential plane (parallel to rolling direction) cracks appear more vertically orientated down to the core, whereas in the axial plane (perpendicular to rolling direction) cracks are more parallel to surface with less vertical branches being observed [25–28].

Despite the amount of research and investigations conducted over decades and the many hypotheses proposed, formation mechanisms of WEC are still not confirmed, neither are the formation drivers. A number of possible drivers for WEC formation have been suggested in research based on the particular methods used in experiments, for example hydrogen diffusion into bearing steel [23], electrothermal effects [29], transient load and/or speed [30,31] and other drivers [22,32]. Different WEC initiation mechanisms have also been proposed based on specific findings, such as initiating at surface or in subsurface. The surface initiation hypothesis suggests that WECs initiate from damage or microcracks on the surface, which are caused by the ruptures of lubricant film due to high surface stress concentration, and subsequently propagate into subsurface. The subsurface initiation hypothesis suggests that WECs initiate from material defects or stress raisers (e.g. inclusions, voids, large carbides, etc.) in the maximum shear stress region under the bearing contacting surface then network and propagate towards the bearing surface leading to axial cracking or WSF failures. [14,26,33–35]. Due to the complicated three dimensional features, it is extremely difficult to confirm whether a particular WEC network was initiated in subsurface then propagated to the surface or initiated at the surface. Recent research results provided more and more evidence for the subsurface initiation theory through detailed WEC network analysis using serial sectioning methods and X-ray tomography [27,36,37]. A recent review provides a comprehensive overview on the hypotheses for WEC initiation and propagation mechanisms [11].

Microstructurally, WECs are cracks accompanied by a material transformation, called White Etching Area (WEA) that makes it a unique and complex failure mode. The term 'white etching' comes from the white appearance of the microstructure after being etched, typically with Nital or Picral, and observed under Light Optical Microscopy (LOM). It is still unclear whether microcracks or WEAs form first in a WEC or whether it is a cooperative growth of the two. All laboratory WEC investigations have been conducted under some accelerating conditions such as using a 'bad oil' or hydrogen pre-charging or applying current across the contact. Although analyses on failed specimens from both laboratory test rigs and service have been conducted, it is difficult to capture the initiation mechanism of WSF (WEA or microcrack). However, there has been more micrographic evidence of cracks without WEA than WEA without cracks presented in literature [36], which has led to believe that microcracks may form before the formation of WEA adjacent to the cracks [11,38,39]. This has been explained as that, after cracks formed, the crack faces rub against each other under RCF leading to the formation of WEA [15,25,28,32,39–41]. Nevertheless, recent investigations on subsurface initiated WECs have shown to have an irregular DER without any apparent cracks that was suggested to be a premature state of WEC [35].

WEAs associated with WECs have been identified by Selected Area Diffraction Patterns (SADP) as nanocrystalline body centred cubic (bcc) ferrite that is supersaturated with carbon [42–44], however recent Atom Probe Tomography (APT) investigations have shown that carbon is segregated at the grain boundaries rather than in the ferrite grains [45,46], but the level of carbon saturation of ferritic nano-grains in WEA has not been confirmed. Grain sizes within WEAs have been reported to be up to 20–30 nm [41,47], whereas some reported randomly distributed grains between 10 and 300 nm sizes in WEAs [48–50]. Coarser grains have often been found at the boundary between WEA and steel matrix [20]. Recent APT analysis has revealed grains to be equiaxed 10 nm ferrite grains within WEA, whereas the original material has a plate-like martensite structure with carbides [45,46]. Amorphous like structures in WEC have also been reported [47]. The hardness of the WEA has been found to be 30–50% higher than the surrounding matrix, which has been suggested to be related to the ultrafine, nanocrystalline structure and carbon supersaturation in WEA [17,41,44,51–53].

Typical WEA has smooth appearance under LOM, however fine structural features and markings [17,38,50,51,54] as well as voids and cavities within WEA have been observed [34,44,55]. In WEAs of Nital-etched specimens, microcracks have been shown under Scanning Electron Microscope (SEM) imaging with Secondary Electrons (SE) [17,34,41,44,47,55,56]. However a recent study by Diederichs et al. [20] revealed that some of the "microcracks" were in fact elongated grain structures (also called needle-shape grains) and suggested that they were a product of annealing processes in WEA. The elongated grain structures were confirmed by Backscattered Electrons (BSE) imaging in SEM or Electron Backscatter Diffraction (EBSD) with colloidal silica (OP-S) polished specimens (not etched with Nital). It was thus suggested that elongated grains within WEA may have the tendency to be etched more with Nital due to its chemical composition, for example different carbon content, and hence had been interpreted as microcracks. They also found that the elongated grains appeared to grow mostly from the cracks into the WEA with no connections to the crack and have lower misorientation, suggested that recrystallisation might have occurred after the formation of the nanocrystalline WEA [20]. Earlier, Grabulov et al. [44] presented similar EBSD images of WEA from a butterfly, however called them elongated 'lamellar' structures and suggested that they had originated from fragmented martensite lamellas. They did however also show low misorientation in the elongated 'lamellar' structures and proposed that incomplete recrystallisation processes had occurred leading to the dislocation free elongated 'lamellar' structures.

Some researchers have also reported that WEA appears as an area predominantly free from carbides while the adjacent material matrix contains unchanged primary spheroidised carbides [17,20,33,38,48,57,58], while others reported that elongated carbides were observed in WEA [33,38,48,50,51,55,58]. The disappearing and/or elongation of the primary spheroidised carbides in WEA has been suggested as a result of carbide dissolution or breaking up due to severe plastic deformation, increased dislocation interaction and grain refinement; following which, carbon diffuses from carbides into WEA [27,33,36,38,45,46,51,57–60] and segregates at the grain boundaries [46,60].

Diederichs et al. [20] also performed chemical analysis within WEA using Energy-dispersive X-ray Spectroscopy (EDX) maps, where inhomogeneous chromium redistribution in WEA was shown. An increased amount of chromium was observed in regions with the finest grains that correlate with the regions suspected to contain primary spheroidised carbides originally [20]. However further X-ray microanalysis is required to examine the carbon distribution to reveal the mechanism of carbon redistribution at a bigger scale than that of APT.

Different from WECs, DER and WEBs are known to form in bearing steels due to medium to high contact pressure RCF after prolonged cyclic loading towards the end of bearing useful life. DER is a region of deformed microstructure features that appear dark under LOM after being etched. WEBs are a combination of bands that rise towards the surface at an angle of either 30° or 80°, when viewed in the circumferential cut (parallel to rolling direction). Many studies have mentioned and even intended to relate WECs with WEBs, however no detailed comparison have been made in literature. Recently the authors of this paper conducted a detailed study on DER and WEBs subjected to RCF testing and found that the initial microstructure of the AISI 52100 through-hardened

martensitic bearing steel was altered in its chemical composition, phase content, grain size, internal stress and hardness [1], showing some similarities with those in WECs reported in literature. A parallel study on WECs has thus been conducted to further identify correlations between them and DER and WEBs.

This paper presents the results from analogous detailed analyses on the microstructure alterations in WECs using a combination of modern microstructure characterisation techniques similar to those used for the DER and WEBs in [1], including SEM, EBSD, EDX, Transmission Electron Microscopy (TEM), and nanoindentation. A comparison between the WECs and DER/WEBs is given in the discussion section to provide an insight into the relations between these microstructural alterations in the AISI 52100 through-hardened martensitic bearing steel.

2. Experimental details

2.1. WEC specimens and material properties

A cylindrical roller bearing of N216 type removed from the service screw compressor due to inner race surface spalling has been used in this study to investigate microstructural alterations in the bearing steel. The bearing had run for 18,000 h (approximately 4628 million cycles) at a rotating speed of 4285 rpm and was lubricated with PAO 68 oil (ISO VG 68, kinematic viscosity 60–70 mm^2/s). The width, inner and outer diameter of the N216 bearing was 26, 80, and 140 mm respectively.

The bearing was manufactured from standard through-hardened AISI 52100 (also known as 100Cr6, SAE 52100) bearing steel that had been subjected to a standard heat treatment process including austenitisation at 830–860 °C and quenched in oil to 60 °C, followed by tempering at 170–220 °C for 2 h. The steel has a typical microstructure consisting of tempered martensite with homogeneously distributed primary spheroidised carbides (Fe, $Cr)_3C$, tempered carbides and approximately 10–12% retained austenite. The chemical composition of the steel is shown in Table 1, analysed by Sheffield Assay Office using an inductively coupled plasma optical emission spectrometry. The elements carbon and sulphur were determined using combustion analysis.

2.2. Microstructural characterisation methodology

Specimens from circumferential and axial cuts were obtained near the spalled area on the inner race where an extensive WEC network was observed in the subsurface. Only results from the circumferential cut (parallel to rolling direction) are presented here since same microstructural variations have been observed in the axial cut specimen.

After cutting, the specimen was hot mounted in Bakelite resin followed by grinding and polishing starting from 3 μm, to 1 μm then 0.25 μm diamond suspensions. OP-S was used as the final preparation step to achieve a deformation-free surface for obtaining orientation contrasts in the BSE images in SEM and EBSD analyses.

The prepared surface was firstly examined using BSE imaging performed under conditions favourable for orientation contrast observation. This is a relatively new technique in the field of the WEC investigations [20], where complex microstructural variations within the WEC can be observed without chemical etching artefacts. Following BSE imaging, EBSD was performed to examine the structure, phase of the material, crystal orientation and misorientation in WECs. Even though EBSD has been widely used as microstructure characterisation technique, it has not been frequently applied in WEC analysis [20,44]. After BSE and EBSD analyses, the surface of the specimens was slightly re-polished to remove the contamination layer from the BSE and EBSD analyses then etched with 1% Nital solution (1 ml HNO_3, 99 ml Ethanol) for 1–3 s prior to be imaged using LOM (Olympus BX51) and SE SEM, which are two typical techniques used in WEC research. The SEM used for this study is a JEOL JSM 7000F field emission gun microscope equipped with a combined EDAX Pegasus EDX/EBSD system.

The BSE and SE SEM investigations were performed at an accelerating voltage of 10 kV with approximately 5 mm and 10 mm Working Distance (WD) respectively. EBSD investigations were performed at an accelerating voltage of 15 kV and a probe current of 30–35 nA under WD of 15–17 mm with step size of 50 nm.

The EBSD data have been evaluated with EDAX OIM 7.3. For indexing purposes the phases of α-Fe, γ-Fe and Fe_3C were chosen. In most of the evaluations, the data have been evaluated without additional data clean-up, only for analysis of the grain boundaries a moderate clean-up by neighbour Confidence Index (CI) correlation has been performed prior to the evaluation to avoid the data points with CIs less than 0.1.

Selected WEC areas have been further analysed by TEM. The TEM specimens were prepared using a Focused Ion Beam (FIB) (FEI Strata 205) with a tungsten layer deposition for surface protection. The milling was performed at an acceleration voltage of 30 kV with current from 20.2 nA down to 3.49 pA. The cut lamellae were placed onto a copper grid for imaging. TEM bright and dark field imagining and SADP were obtained with a FEI Tecnai F20, operating at 200 kV.

Nanohardness tests were also performed on various areas of the WEC using a computer-controlled hardness measuring system (Fischerscope H100C, Helmut Fischer GmbH, Sindelfingen). Indentations were made in force control mode by applying a force of 10 mN. A fixed loading/unloading rate of 0.5 mN/s and a dwell time at maximum load of 5 s were used for all hardness measurements in this study. After indentation all the indents were imaged by SEM to examine the indents and analyse the results. For the steel matrix, the hardness of an average of 26 indents was achieved. However, for the heterogeneously altered microstructures, averaging is not appropriate due to the variations at different features, therefore the results of individual indents are presented.

3. Results

The microstructural variations observed in the WEC using a range of advanced techniques are firstly presented in this section, which are then compared with those found in DER and WEBs [1].

3.1. Light Optical Microscopy (LOM)

Fig. 1 shows a LOM image of a WEC network found in the subsurface of the bearing raceway that has been examined in this study. The section of the WEC shown in this image appears to have no connection to the surface and it extends from approximately 50 μm to 600 μm below the contact surface.

Table 1
Chemical composition of the AISI 52100 bearing material analysed by Sheffield Assay Office, wt%.

C	Cr	Si	Cu	Mn	Al	P	Co	Zn	S	Sn	Ni	Mo
0.944	1.65	0.20	0.20	0.37	0.03	<0.01	<0.01	<0.01	0.005	0.01	0.16	0.03

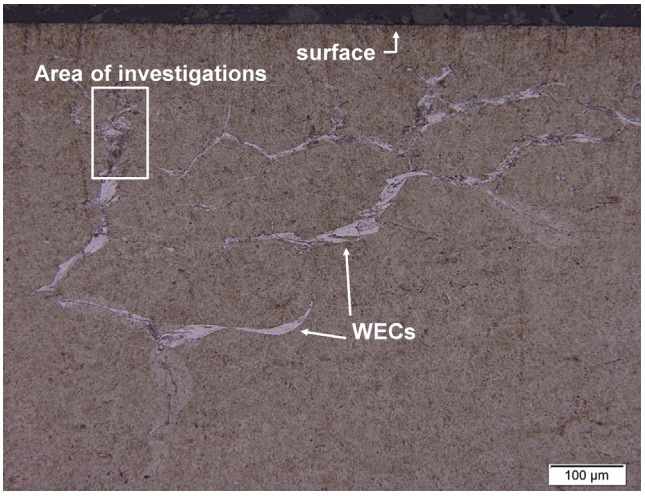

Fig. 1. LOM micrograph of WECs in circumferential cross-section (Nital-etched). The area of further investigations is marked with a rectangle.

3.2. Scanning Electron Microscopy (SEM)

An area (marked by the rectangle in Fig. 1) of the WEC network has been chosen to be examined under SEM with SE and BSE imaging to reveal microstructural changes in the WEC and the results are shown in Fig. 2. Extensive microstructure alterations are seen with only relatively small microcracks detected by the BSE SEM imaging on OP-S polished specimen (marked with white arrows in Fig. 2(a) and (b)). It is also evident that the WEA consists of four other distinct constituents, including coarse, fine, nanocrystalline and elongated grains marked in both the SE and BSE SEM images. As discussed above, the elongated dark features, appeared as deep grooves in the SE SEM (Nital etched), are clearly shown as elongated grains in BSE SEM (OP-S polished) shown in Fig. 2, where selected areas of elongated grains are marked with red arrows. The elongated grains inside the WEA appear in the middle or close to the edge of the WEA. While groups of paralleled elongated grains are seen, a uniform direction of grain growth comparable to the directional growth during RCF has not been observed. Different size grains in the WEA appear to be randomly distributed and do not have any correlation with the crack or other features in the WEC. No primary spheroidised carbides are observed in the WEC area.

3.3. Electron Backscattered Diffraction (EBSD) and energy dispersive X-ray spectroscopy (EDX)

Fig. 3 shows EBSD and EDX maps of the selected region shown in Fig. 2, including an Image Quality (IQ) map (Fig. 3(a)), a map displaying the non martensite-martensite High Angle Grain Boundaries (HAGBs) (Fig. 3(b)), a chromium EDX map (Fig. 3(c)) and carbon EDX map (Fig. 3(d)). The nanocrystalline regions of the WEA are usually too fine to produce a good EBSD pattern, therefore they appear dark in the IQ map shown in Fig. 3(a). However, the large regions of coarser globular and elongated grains embedded within these nanocrystalline areas are showing comparatively high IQ values, suggesting that these grains were newly formed and of ferritic structure. Fig. 3(b) depicts the HAGBs found in this region, which are not predicted by the usual orientation relation models of the martensitic transformation developed by Kurdyumov-Sachs [61], Nishiyama-Wassermann [62], Greninger-Troiano [63] and Pitsch [64]. In the unaltered steel matrix, these grain boundaries correspond only to the boundaries of the equiaxed prior austenite grains. Around the WEC, however, a large amount of newly formed HAGBs, which do not have their origin in a martensitic transformation, are found. The overall extension of these HAGBs clearly coincides with the size of the microstructurally altered region.

For comparison, the chromium and carbon distributions measured by EDX during the EBSD scan in the energy ranges of Cr-Kα and C-Kα are shown in Fig. 3(c) and (d). In the unaltered matrix, primary carbides are clearly shown as higher X-ray intensities in both Cr-Kα and C-Kα energy ranges. In comparison, in the microstructurally altered region, no similar high intensity spots are seen. In the chromium map, the altered area shows more or less homogeneous intensities. In the carbon map some high-intensity areas within the altered region are detected and the average intensity in the altered area is slightly lower than that in the unaltered matrix. Since the detection of low energy X-rays is challenging at the scanning speed of an EBSD scan, the maps appear to be noisy and the count rates can only be evaluated statistically. A 13% drop for carbon and a 3% drop for chromium have been found by comparing the accumulated X-ray intensities over areas of 10 µm by 10 µm around positions 1 and 2 marked in Fig. 3(d). In order to understand the causes of the inhomogeneous carbon intensities within the altered region, TEM analysis has been conducted on lamellae cut along the red lines shown in Fig. 3(d).

From the EBSD scans, a Kernel Average Misorientation (KAM) map has been obtained (see Fig. 4) to get more details about the misorientations in the indexed part of the WEA. It can be seen that the equiaxed grains and elongated grains have slightly lower misorientations than those in the initial matrix. Together with the HAGBs shown in Fig. 3(b), it is suggested that recrystallisation have taken place in the WEA. The dark/black regions appeared in Fig. 4 are areas of the unindexed WEA, where the grains are too small to give unambiguously indexable EBSD patterns (CI < 0.1).

Inverse Pole Figure (IPF) maps of the area of interest with respect to the rolling normal direction are plotted in Fig. 5 for: all points indexed with CI more than 0.1 (Fig. 5(a)); bcc grains in altered region with grain size less than 250 nm (Fig. 5(b)); and bcc grains in altered region with grain size more than 300 nm and aspect ratio less than 0.5 (Fig. 5(c)). The indexable crystallites within the altered region appear to be present in clusters of preferred orientations, which, however, do not show any correlation with the prior austenite grains of the martensitic matrix, see Fig. 5(a). The altered microstructure is separated into small rather globular grains and larger elongated grains as seen in Fig. 5 (b) and (c), respectively. Both components show similarities in the preferred crystal orientation within each cluster but crystal and shape orientation of the elongated grains change from one cluster to another.

3.4. Transmission Electron Microscopy (TEM)

Fig. 6 shows the dark field TEM image and corresponding SADP patterns for the two TEM lamella cuts at the positions shown in Fig. 3(d). D-values and lattice constant for the TEM lamella 2, corresponding to low C-Kα intensity area, have been calculated and have been found to be compatible with a pure iron bcc crystal structure. Similar ring patterns have been reported in literature [38,44,48] for typical WEA. This also agrees with the recent APT results [45,46] which found a carbon segregation with carbon present at grain boundaries rather than in ferrite grains, hence lattice constant is the same as for pure ferrite [46,60]. The intensity distribution within the rings suggests that preferred crystal orientations are present among the nanocrystalline WEA grains, however the particular crystal orientation leading to such a texture has yet to be confirmed.

The SADP of the TEM lamella 1, corresponding to the high C-Kα intensity area, clearly shows additional rings, suggesting a more

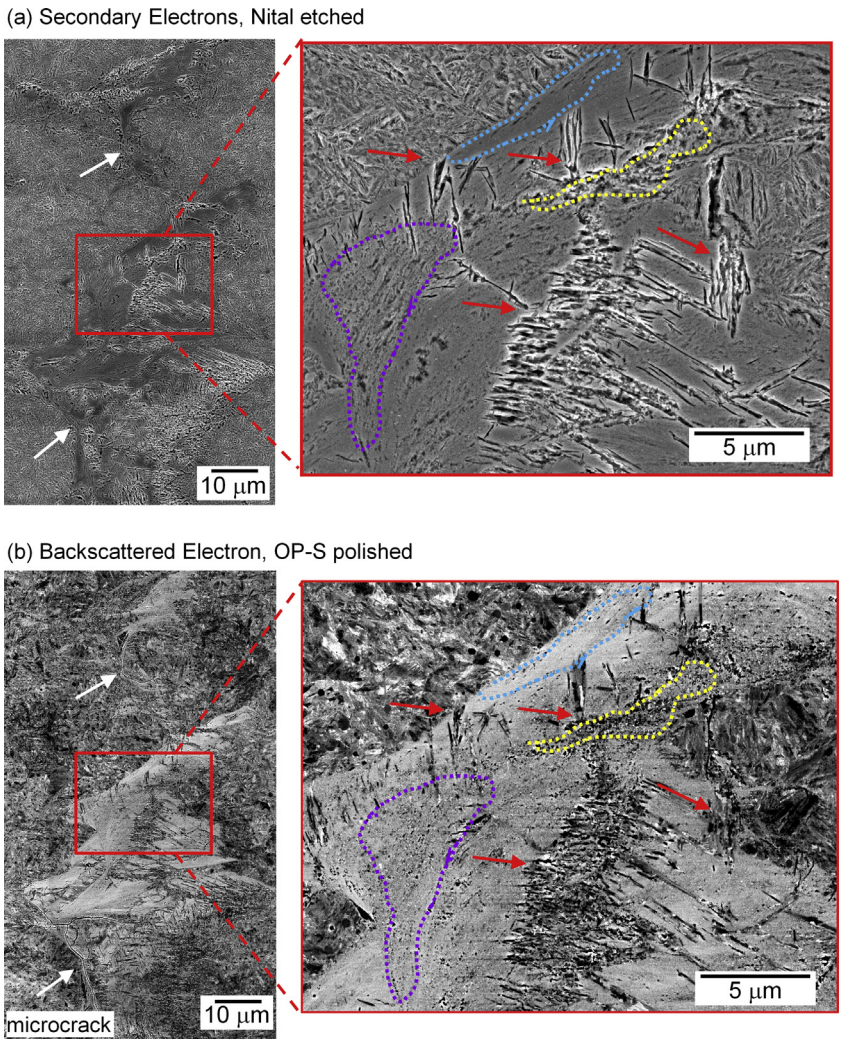

Fig. 2. SEM images of the same area in the WEA attained by: (a) SE imaging in Nital-etched condition; (b) BSE imaging in OP-S polished condition. Examples of coarse, fine, nanocrystalline and elongated grains are marked with yellow, purple, blue dash line and red arrow respectively. Microcracks are marked with white arrow.

complex phase or a mixture of phases in this region. Two different phases have been identified from SADP, corresponding to bcc and hexagonal crystal structures. D-values and intensities of the reflexes corresponding to hexagonal crystal structure match with the space group $P6_3/mmc$ and M_2C crystal structure. This suggests that a mixture of typical WEA and newly formed carbidic structures is present in this area. In contrast to the primary spheroidised carbides in the unaltered matrix, the areas with high C-Kα intensities do not show an elevated chromium content, which also indicates that they are not just ground primary spheroidised $(Fe, Cr)_3C$ carbides, but rather newly formed carbidic structures.

3.5. Nanohardness

Exemplary SEM images of nanoindents in four different regions are shown in Fig. 7. Analysis of multi-nanoindents in unaltered matrix has shown an average hardness of 900 HV0.001 with a standard deviation, σ, of 36 HV0.001. For the altered microstructures, however, each indented position is different, thus individual local hardness values are presented. In the regions with coarse globular and elongated grains (Fig. 7(b)) the material is softer than the unaltered steel matrix (Fig. 7(a)), while in the regions with finer grain (Fig. 7(c)) and especially with the nanocrystalline structures (Fig. 7(d)) the materials are considerably harder than the unaltered martensitic matrix. All three reported values differ more than 3σ from the average matrix hardness and have to be considered as significant.

4. Discussions

4.1. WEC features discussions

In addition to the features reported in literature, this study has revealed that the analysed part of the WEC contains relatively small microcracks with extensive microstructural alterations, such as WEAs, elongated and varied size grains, which are typically located on one side of the WEC. The relatively big altered area with small microcracks and the fact that the microstructure alteration only appears on one side of the crack suggest that the microstructural transformation does not occur due to rubbing of the crack faces [25,32,39]. Although it could be possible that microcracks formed initially, led to microstructure alteration due to face rubbing then closed under pressure, it has not been possible to confirm if or at which point what happened, since the analysis has been conducted on fully developed WECs. A time-resolved analysis on WEC formation is currently conducted to further investigate these issues.

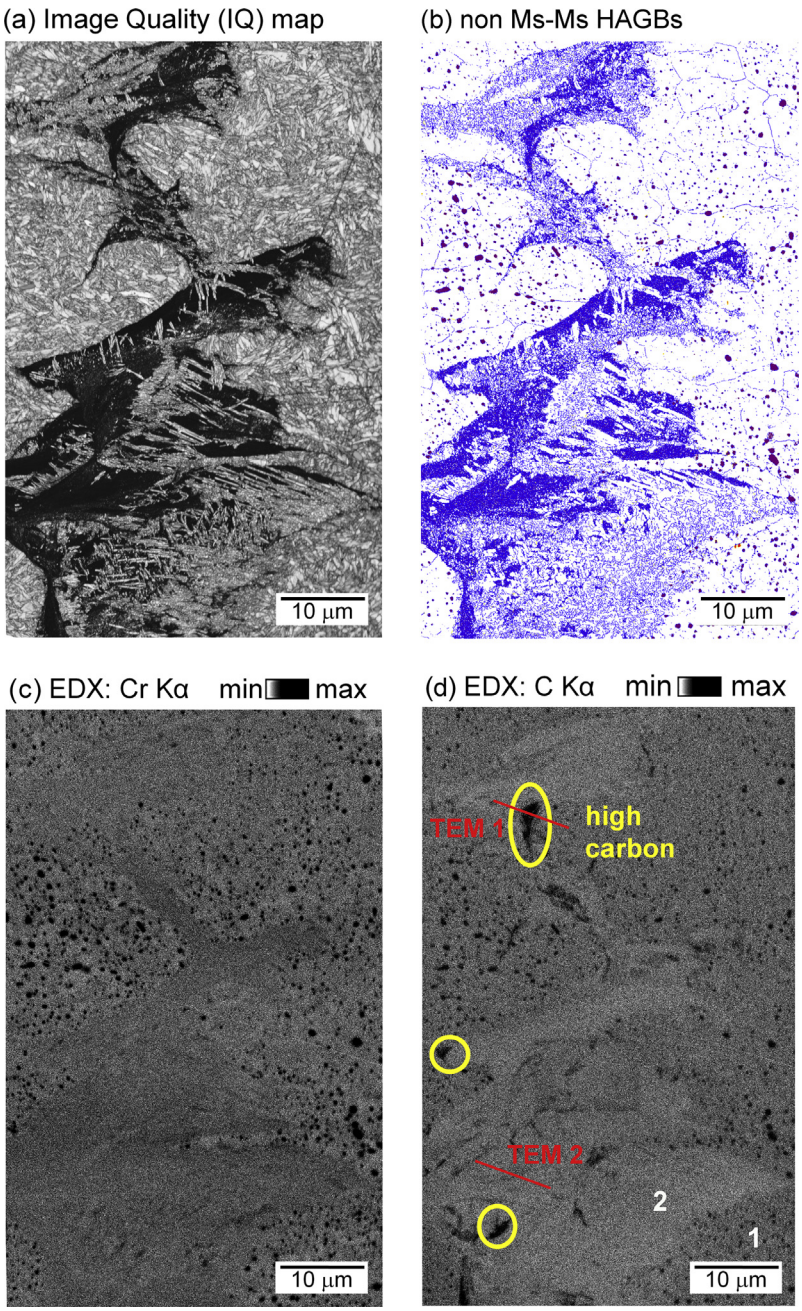

Fig. 3. EBSD/EDX maps of the WEA: (a) IQ map; (b) non martensite-martensite HAGBs map; (c) chromium map; (d) carbon map with marked carbon-rich areas, positions of the TEM lamellae, and positions '1' and '2' discussed in the text.

Scepanskis et al. [29] suggested that localised resistivity heat causes thermal expansion and localised stresses at the interface between carbides and steel matrix leading to the microstructure alteration. Their theory was based on the fact that carbides have the lowest conductivity properties compared to bainitic and martensitic structures in steels and thus could be overheated and suffer plastic deformation resulting in dissolution and carbon diffusion, initiating WEA formation. It was also suggested that the thermal effect could create material defects (e.g. voids) or cause temperature variation in materials that potentially promotes the growth of elongated grains observed in this and other studies [20].

This study has shown that the WEA microstructure consists of multiple constituents including globular grains of various sizes and elongated grains (Fig. 2). Irregular zones of coarser grains and elongated (needle-shape) grains in WEAs from vacuum pump bearings have also been reported previously [20], where elongated grains were found to grow preferentially from the crack into the altered region. It was proposed that elongated grains grow as a result of a higher temperature due to internal friction and plastic deformation at the vicinity of cracks [20]. In this study, however, elongated grains have been seen in the altered regions: in the middle and close to boundaries of the material matrix. This suggests that different causes for the growth of elongated grains may exist. The findings on the low misorientation of the globular and elongated grains in combination with the occurrence of new non-martensitic HAGBs from this study suggest that recrystallisation processes have occurred at some point during the microstructural alteration process. It is however difficult to explain the formation of the elongated grains, but it can be seen that the clustered crystal orientations differ from the appearance of the martensitic

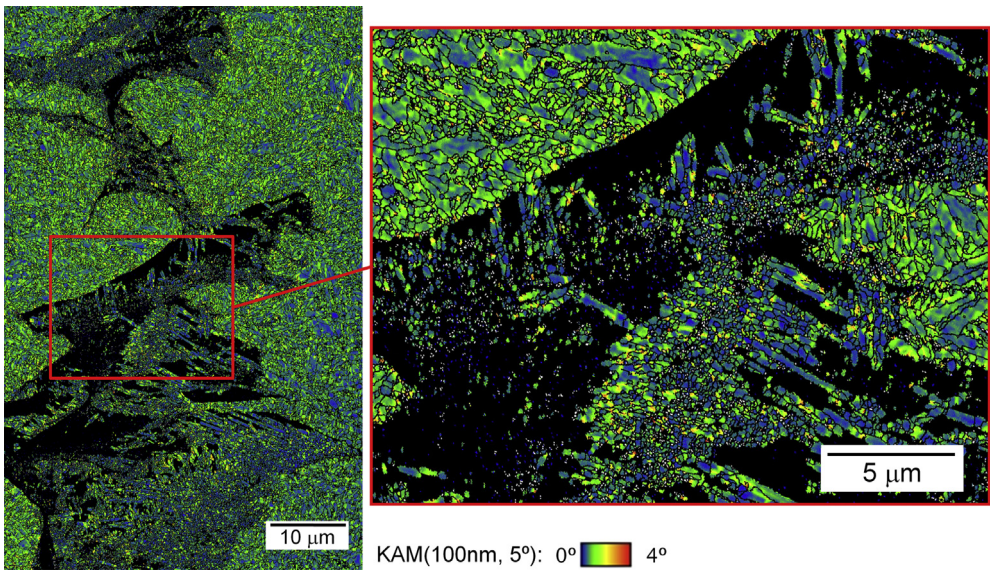

Fig. 4. An EBSD KAM map of WEA for the points indexed as α-Fe, γ-Fe and $(Fe,Cr)_3C$ carbides with CI > 0.1. Step size 50 nm.

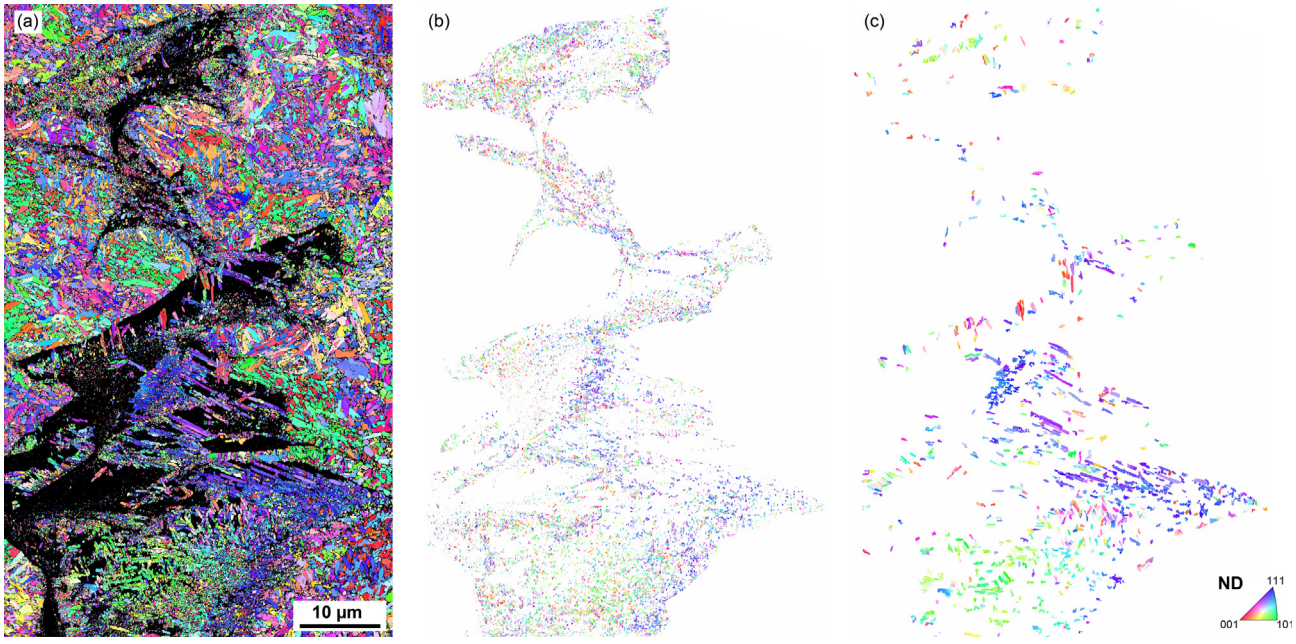

Fig. 5. IPF maps with respect to the rolling normal direction: (a) all points indexed with CI > 0.1; (b) bcc grains in altered region with grain size <250 nm; (c) bcc grains in altered region with grain size >300 nm and aspect ratio <0.5.

microstructure. For example comparing the size of the blue/green clusters of elongated grains in the lower part of the altered region in Fig. 5(a) with the typical size of the prior austenite grains (indicated in the unaltered matrix regions of Fig. 3(b)) clearly show that the elongated grains are not just isolated martensite laths remaining from the dissolving initial microstructure. Such elongated grains have also been misinterpreted as defects or microcracks under SEM of Nital-etched samples in many of previous studies [17,34,41,44,47,55,56].

4.2. WECs vs. DER and WEBs

In this section, the WEC features found in this study are compared with those found in DER and WEBs due to high-stress RCF [1] to understand the differences and correlations between WECs, DER and WEBs in rolling bearings, providing links in the microstructure transformation and derive drivers for the currently unpredictable WEC failure.

Similar globular and elongated ferritic grains seen in the WEC have been also observed in DER and WEBs in AISI 52100 through-hardened martensitic bearing steel specimens subjected to high-stress RCF testing [1]. However, different from the DER and WEBs, where the crystal orientations of the newly formed grains were found to be lying in a {1 1 2} plane, the elongated grains in the WEC network do not show any uniform local orientation that can be directly related to the external rolling conditions. The prevailing texture of the newly formed ferritic grains in the WEC varies from cluster to cluster in the WEC network. The

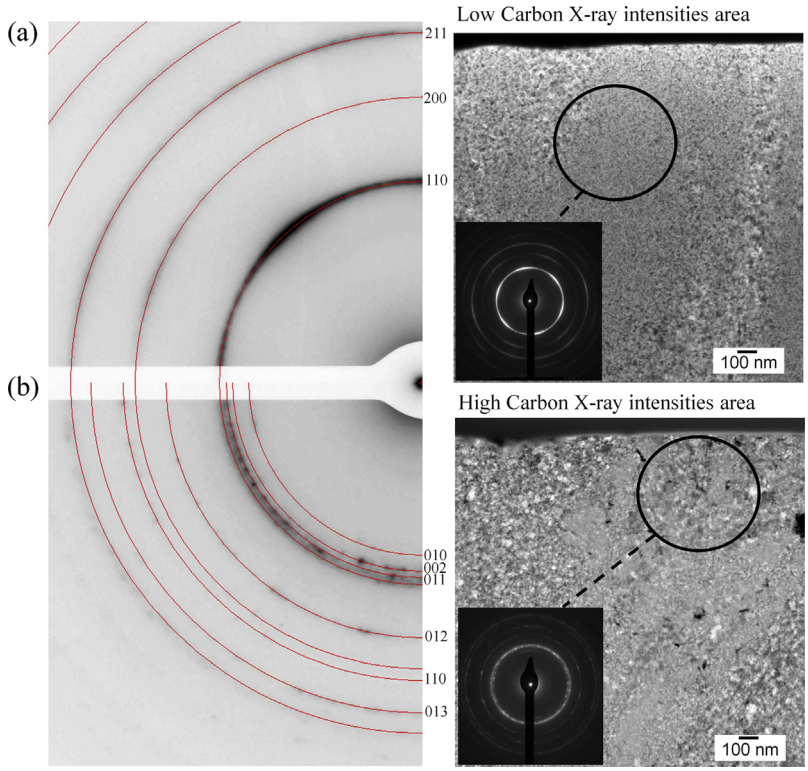

Fig. 6. Dark field TEM images and corresponding SADP of: (a) low carbon X-ray intensity area in the WEA (TEM 2) with typical bcc ring pattern; (b) high carbon X-ray intensity area in the WEA (TEM 1) with ring pattern showing mixture of bcc and hexagonal crystal structures.

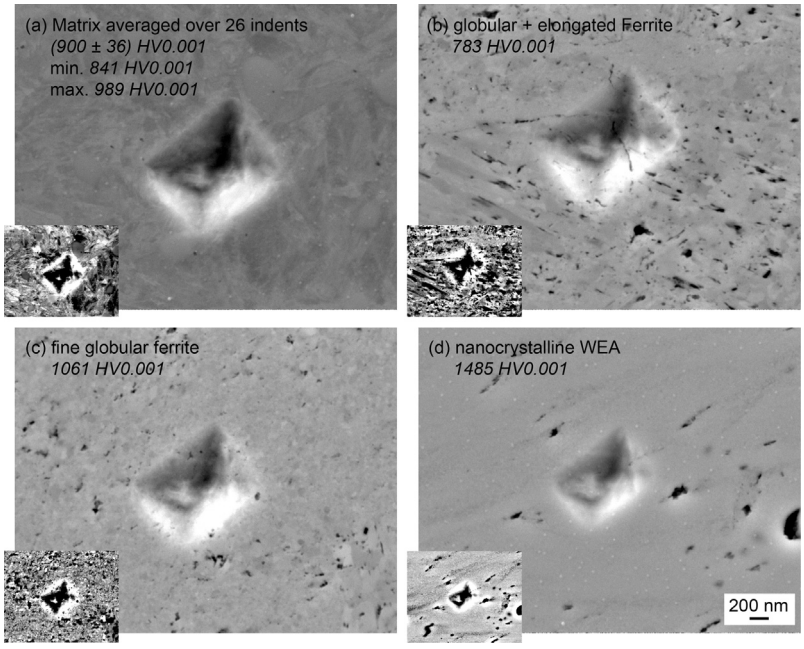

Fig. 7. Nanohardness indents with an applied force of 10 mN into the different microstructural components. Large images: SE images, small images: orientation contrast BSE images of the same region.

elongated grains in the WEC show a similar crystal orientation (Fig. 5(b)) as those of the smaller globular grains (Fig. 5(c)), suggesting that they have similar formation mechanism.

Primary spheroidised carbides have been found to be absent in both WECs [27,33,36,38,45,46,51,57–59] and WEBs [1,57,65–67]. This has been considered to be caused by carbide dissolution or breaking up due to severe plastic deformation, increased dislocation interaction, or grain refinement. Through the EDX analysis, redistribution of chemical elements especially the homogenisation of chromium has been observed in both WEC and WEBs [1]. However, Diederichs et al. [20] have previously shown a chromium redistribution in WEC where higher chromium concentration was

seen close to the location of former primary spheroidised carbides. This has led to believe that the chromium may have had sufficient time to diffuse and incorporate into the bcc lattice of the newly formed grains in the WEC studied here to show a homogeneous chromium distribution.

As for the carbon redistribution, even though the measurement of carbon is generally challenging using EDX, the corresponding X-ray map obtained shows an inhomogeneous carbon redistribution within the microstructurally altered regions in both the WEC and WEBs [1]. The high carbon intensities found for the primary spherical $(Fe, Cr)_3C$ carbides in the unaffected matrix of the WEC and WEBs specimens are not seen within the altered region, suggesting that not only the decomposition of the crystal structure has occurred but also a movement of the elements enriched in the former primary spheroidised $(Fe, Cr)_3C$ carbides. It is interesting that elevated carbon intensity is only seen at particular locations of the altered region in the WEC specimen, often at the boundaries of the altered region. Similar high carbon intensity areas, that are strongly resistant to etchant and result in EBSD unindexable regions, have also been observed in the WEBs specimen where carbon appeared to have moved from ferritic microstructure of the 80° bands and accumulated between the globular regions of the 30° bands and close to the corners where 30° and 80° features intersect [1]. The size of the high carbon intensity areas is larger than the size of typical primary spheroidised $(Fe, Cr)_3C$ carbides and the fact that the concentration of chromium is shown to be homogeneous in such areas, suggests that primary spheroidised $(Fe, Cr)_3C$ carbides must have been disintegrated completely while sufficient time has been available for chromium to diffuse and homogenise in the transformed microstructure. Furthermore, the comparison of accumulated carbon intensities in larger areas of 1 and 2 marked in Fig. 3(d) shows slightly lower intensities for the altered region (marked as 2) compared to the unaltered steel matrix (marked as 1). This is contrary to the results from an APT analysis, where total carbon in a WEA is similar or higher than that in an unaffected matrix [45]. However, the area analysed using APT was extremely small and the position of APT samples was chosen based on the appearance of the area in the etched condition, in which high and low carbon X-ray intensity areas could hardly be distinguished [45]. Furthermore, if the accumulated carbon intensities in the marked areas (1 and 2 in Fig. 3(d)) indicate a possible net loss of carbon in the altered regions during the formation of the WEA or just a redistribution bringing the local carbon concentration closer to the EDX detection limit, cannot be confirmed conclusively with the present data. Further analysis is thus required to clarify the carbon movement during WEA formation.

The unique feature that has been seen in WEC but not in WEBs is the nanocrystalline material with grains at about 10 nm sizes observed in the TEM. Whereas the TEM analysis of the low carbon intensity position yielded the typical nanocrystalline bcc structure, the corresponding analysis of the elevated carbon intensity area in the WEC shows a mixture of the nanocrystalline bcc and newly formed M_2C structures therefore reconfirms the differences observed in the EDX carbon map. This mixture of two nanocrystalline phases in WEC is different to the crystal structure of high carbon intensity areas seen in the WEBs [1] that is a complex but not nanocrystalline structure.

Hardness heterogenisation has been observed in the WEC specimens for the first time in this study through the nanohardness analyses (Fig. 7). The hardness in regions of fine globular grains and nanocrystalline areas is found to be considerably higher than that in the steel matrix. However, in regions with coarser globular and elongated grains, the material is found to be softer than the initial matrix. Similar hardness variations were observed in WEBs, where areas with high carbon X-ray intensities appear to have higher hardness, whereas globular and elongated grains have lower hardness than the original steel matrix [1]. The hardness variations observed seems to be related to phase, grain size variation and carbon concentration in the relevant microstructural features.

Furthermore the loading conditions for WEC are found to very different from those for DER and WEBs formations especially in laboratory recreation testing. In addition to the normal loading conditions for DER and WEBs creation, additional loading such as electrical [29], chemical [24,68] or others as well as environmental conditions have been used to initiate WECs in laboratories. With pure and excessive mechanical loading, the AISI 52100 through-hardened martensitic bearing steel typically fails with the formation of the DER and WEBs. The additional loading and/or environmental conditions must have caused the nanocrystalline material and crack formation in WECs resulting in bearings fail at much earlier stage of their lives due to WSF.

Non-metallic inclusions and other stress raisers (e.g. voids, large carbides etc.) in the maximum shear stress region under bearing surfaces have been proposed to be a driver for WEC formation [14,26,33–35]. This contradicts the fact that DER and WEBs without cracks form under much higher stress conditions than that for WECs in the same AISI 52100 through-hardened martensitic bearing steel with similar cleanliness or contents of stress raisers. To further investigate this issue studies on evolution of WECs are currently undertaken by the authors of this study, where early stages of WECs in addition to the fully developed WECs are fully analysed.

5. Conclusions

Using a combination of SEM, EBSD, EDX, TEM and nanoindentation techniques, this study has provided detailed analyses on WEC microstructure transformation in AISI 52100 through-hardened martensitic steel. Further from the study conducted by Diederichs et al. [20], this investigation focuses on detailed analysis of the complex microstructure in WECs and provides a comparison between the microstructure alterations in WEC and those in DER and WEBs due to RCF also studied by the authors of this paper [1]. The main conclusions from this study are:

- Elongated and globular grains at various sizes have been observed in WECs. The elongated grains appeared within the altered region of the WEC as well as at the boundary between material matrix and the altered regions. Similar elongated and globular grains have also been observed in DER and WEBs. In contrast, the elongated grains in WEBs have a defined growth direction related to the rolling direction, whereas those in WECs are locally defined in clusters without a global direction that can be related to the rolling conditions.
- No primary spheroidised carbides $(Fe, Cr)_3C$ have been observed in WECs or WEBs [1], suggesting that they are likely to have experienced similar stages of the microstructure alteration processes. Dissolution of primary spheroidised carbides is shown in the redistributions of carbon and chromium in the altered areas.
- Inhomogeneous carbon redistribution within the WEC network is observed in the EDX carbon map where randomly distributed localised high carbon intensity areas are also shown. While similar carbon-rich areas were observed in WEBs, these areas appeared to be crystallographically different from those in WECs under TEM investigations.
- A hardness heterogenisation within the WEC has been detected using nanoindentation measurements. It was found that the hardness in regions with fine globular grains and nanocrystalline structures are higher than the unaltered steel matrix, whereas the regions with coarser globular and elongated grains

have nanohardness lower than the unaltered steel matrix. Similar hardness heterogenisation was observed in DER and WEBs, where the regions with globular and elongated ferritic grains have lower nanohardness and the regions with high carbon intensity have higher nanohardness compared with the unaltered steel matrix.

Although the studies have clearly shown that the microstructure transformation in WEC has many similarities with those in DER and WEBs under the identical examination procedure, the causes of the distinguishing nanocrystalline structure in the WECs that subsequently leads to the much earlier WSF bearing failures as compared to the high-stress cycle RCF are still unclear. Further investigations are being conducted on bearings tested at varied durations to study evolution of the microstructure alterations in WECs. APT will be employed to identify chemical movements and redistributions in areas with different features (e.g. elongated and globular grains, high and low carbon intensity areas) in order to understand the microstructural transformation processes.

Acknowledgments

Authors would like to acknowledge Basic Tribology, Competence Centre Surface Technology and Schaeffler Technologies AG & Co. KG, Germany, for providing technical supports including bearing samples and valuable suggestions to this study. We also extend our sincere gratitude to colleagues Kevin Kistermann, Martina Schiffers, Sebastian Zischke and Prof. Thomas E. Weirich at GFE RWTH Aachen University for their help in sample preparation and TEM analyses.

This research has been co-funded by EPSRC (project number EP/M50662X/1) and the Competence Centre Surface Technology at Schaeffler Technologies AG & Co. KG.

References

[1] Šmeļova V, Schwedt A, Wang L, Holweger W, Mayer J. Electron microscopy investigations of microstructural alterations due to classical rolling contact fatigue (RCF) in Martensitic AISI 52100 bearing steel. Int J Fatigue 2017;98:142–54. http://dx.doi.org/10.1016/j.ijfatigue.2017.01.035.
[2] McKenna R, Ostman v.d. Leye P, Fichtner W. Key challenges and prospects for large wind turbines. Renew Sustain Energy Rev 2016;53:1212–21.
[3] Kumar Y, Ringenberg J, Depuru Soma S, Devabhaktuni VK, Lee Jin W, Nikolaidis E, et al. Wind energy: trends and enabling technologies. Renew Sustain Energy Rev 2016;53:209–24.
[4] Jain S, Hunt H. A dynamic model to predict the occurrence of skidding in wind-turbine bearings. In: Journal of physics: conference series. p. 1–10.
[5] Ribrant J, Bertling L. Survey of failures in wind power systems with focus on Swedish wind power plants during 1997–2005. IEEE transactions on energy conversion, vol. 22. p. 167–73.
[6] NREL. Statistics show bearing problems cause the majority of wind turbine gearbox failures, U.S. Department of Energy & National Renewable Energy Laboratory (NREL) [Online]. Available: <https://energy.gov/eere/wind/articles/statistics-show-bearing-problems-cause-majority-wind-turbine-gearbox-failures> [accessed 25 Jan 2017].
[7] Hyde S. Improving gearbox reliability by analyzing axial cracking on bearings and recommending a solution, 2012.
[8] Evans MH. White structure flaking (WSF) in wind turbine gearbox bearings: effects of 'butterflies' and white etching cracks (WECs). Mater Sci Technol 2012;28:3–22.
[9] McVittie D. Wind turbine gearbox reliability: the nature of the problem. Gear Engineers; 2006.
[10] Tavner PJ, Xiang J, Spinato F. Reliability analysis for wind turbines. Wind Energy 2007;10:1–18.
[11] Evans MH. An updated review: white etching cracks (WECs) and axial cracks in wind turbine gearbox bearings. Mater Sci Technol 2016;32:1133–69.
[12] Harris TA. Rolling bearing analysis. 3rd ed. New York: Wiley; 1991.
[13] Kang J. Mechanisms of microstructural damage during rolling contact fatigue of bearing steels. University of Cambridge; 2014.
[14] Davies WJ, Day KL. Surface life bearings for automotive alternator applications. Inst Mech Eng 1963:23–40.
[15] Stadler K, Studenrauch A. Premature bearing failures in wind gearboxes and white etching cracks (WEC). Evolution – business and technology magazine from SKF; 2013.
[16] Stadler K. Premature wind gearbox bearing failure. In: NREL GRC meeting.
[17] Greco A, Sheng S, Keller J, Erdemir A. Material wear and fatigue in wind turbine systems. Wear 2013;302:1583–91.
[18] Olver AV. The mechanism of rolling contact fatigue: an update. Proc Inst Mech Eng, Part J: J Eng Tribol 2005;219:313–30.
[19] Murakami Y, Takemura H, Fujii A, Furumura K. Rolling contact fatigue life under contaminated lubrication with several foreign particles. NSK Tech J 1993;655:17–24.
[20] Diederichs AM, Schwedt A, Mayer J, Dreifert T. Electron microscopy analysis of structural changes within white etching areas. Mater Sci Technol 2016;32:1683–93.
[21] Holweger W. White etching cracks. In: NREL wind turbine tribology seminar, Argonne, IL, USA.
[22] Gould B, Greco A. Investigating the process of white etching crack initiation in bearing steel. Tribol Lett 2016;62:1–14.
[23] Ruellan A, Kleber X, Ville F, Cavoret J, Liatard B. Understanding white etching cracks in rolling element bearings: formation mechanisms and influent tribochemical drivers. Proc Inst Mech Eng Part J-J Eng Tribol 2015;229:886–901.
[24] Holweger W, Wolf M, Merk D, Blass T, Goss M, Loos J, et al. White etching crack root cause investigations. Tribol Trans 2015;58:59–69.
[25] Vegter RH, Slycke JT. The role of hydrogen on rolling contact fatigue response of rolling element bearings. J ASTM Int 2010;7.
[26] Evans MH, Richardson AD, Wang L, Wood RJK, Goss M, Loos J, et al. Serial sectioning investigation of butterfly and white etching crack (WEC) formation in wind turbine gearbox bearings. Wear 2013;302:1573–82.
[27] Evans MH, Wang L, Jones H, Wood RJK. White etching crack (WEC) investigation by serial sectioning, focused ion beam and 3-D crack modelling. Tribol Int 2013;65:146–60.
[28] Ruellan A, Ville F, Kleber X, Arnaudon A, Girodin D. Understanding white etching cracks in rolling element bearings: the effect of hydrogen charging on the formation mechanisms. Proc Inst Mech Eng Part J-J Eng Tribol 2014;228:1252–65.
[29] Ščepanskis M, Jakovičs A, Kaldre I, Holweger W, Nacke B, Diederichs A. The numerical model of electrothermal deformations of carbides in bearing steel as the possible cause of white etching cracks initiation. Tribol Lett 2015;59:1–10.
[30] Bruce T, Long H, Slatter T, Dwyer-Joyce R. Formation of white etching cracks at manganese sulfide (Mns) inclusions in bearing steel due to hammering impact loading. Wind Energy 2016.
[31] Luyckx J. Hammering wear impact fatigue hypothesis WEC/Irwea failure mode on roller bearings. In: NREL wind turbine tribology seminar, Broomfield, CO, USA.
[32] Gould B, Greco A. The influence of sliding and contact severity on the generation of white etching cracks. Tribol Lett 2015;60:13.
[33] Sugino K, Miyamoto K, Nagumo M, Aoki K. Structural alterations of bearing steels under rolling contact fatigue. Trans Iron Steel Inst Jpn 1970;10:98–111.
[34] Evans MH, Richardson AD, Wang L, Wood RJK. Effect of hydrogen on butterfly and white etching crack (WEC) formation under rolling contact fatigue (RCF). Wear 2013;306:226–41.
[35] Diederichs AM, Barteldes S, Schwedt A, Mayer J, Holweger W. Study of subsurface initiation mechanism for white etching crack formation. Mater Sci Technol 2016:1–9.
[36] Evans MH, Richardson AD, Wang L, Wood RK, Anderson WB. Confirming subsurface initiation at non-metallic inclusions as one mechanism for white etching crack (WEC) formation. Tribol Int 2014;75:87–97.
[37] Greco A. White etching crack failure overview, tomography analysis, and test development. In: NREL wind turbine tribology seminar. Argonne National Laboratory; 2014.
[38] West OHE, Diederichs AM, Alimadadi H, Dahl KV, Somers MAJ. Application of complementary techniques for advanced characterization of white etching cracks. Praktische Metall-Pract Metallogr 2013;50:410–31.
[39] Bhadeshia H, Solano-Alvarez W. Critical assessment 13: elimination of white etching matter in bearing steels. Mater Sci Technol 2015;31:1011–5.
[40] Solano-Alvarez W, Bhadeshia HKDH. White-Etching matter in bearing steel. Part II: distinguishing cause and effect in bearing steel failure. Metall Mater Trans Phys Metall Mater Sci 2014;45A:4916–31.
[41] Gegner J. Tribological aspects of rolling bearing failures. INTECH Open Access Publisher; 2011.
[42] Martin J, Borgese S, Eberhardt A. Microstructural alterations of rolling—bearing steel undergoing cyclic stressing. J Fluids Eng 1966;88:555–65.
[43] O'Brien JL, King AH. Electron microscopy of stress-induced structural alterations near inclusions in bearing steels. J Fluids Eng 1966;88:568–71.
[44] Grabulov A, Petrov R, Zandbergen HW. Ebsd investigation of the crack initiation and TEM/FIB analyses of the microstructural changes around the cracks formed under rolling contact fatigue (RCF). Int J Fatigue 2010;32:576–83.
[45] Li YJ, Herbig M, Goto S, Raabe D. Atomic scale characterization of white etching area and its adjacent matrix in a martensitic 100cr6 bearing steel. Mater Charact 2017;123:349–53.
[46] Danielsen HK, Guzmán FG, Dahl KV, Li YJ, Wu J, Jacobs G, et al. Multiscale characterization of white etching cracks (WEC) in a 100cr6 bearing from a thrust bearing test rig. Wear 2017;370–371:73–82.
[47] Harada H, Mikami T, Shibata M, Sokai D, Yamamoto A, Tsubakino H. Microstructural changes and crack initiation with white etching area formation under rolling/sliding contact in bearing steel. ISIJ Int 2005;45:1897–902.

[48] Evans MH, Walker JC, Ma C, Wang L, Wood RJK. A FIB/TEM study of butterfly crack formation and white etching area (WEA) microstructural changes under rolling contact fatigue in 100cr6 bearing steel. Mater Sci Eng Struct Mater Prop Microstr Process 2013;570:127–34.
[49] Errichello R, Budny R, Eckert R. Investigations of bearing failures associated with white etching areas (WEAs) in wind turbine gearboxes. Tribol Lubr Technol 2014;70:1069–76.
[50] Kang JH, Hosseinkhani B, Williams CA, Moody MP, Bagot PAJ, Rivera-Diaz-del-Castillo PEJ. Solute redistribution in the nanocrystalline structure formed in bearing steels. Scripta Mater 2013;69:630–3.
[51] Scott D, Loy B, Mills GH. Paper 10: metallurgical aspects of rolling contact fatigue. Proceedings of the institution of mechanical engineers, conference proceedings, vol. 181. p. 94–103.
[52] Lund TB. Sub-surface initiated rolling contact fatigue-influence of non-metallic inclusions, processing history, and operating conditions. J ASTM Int 2010;7:1–12.
[53] Osterlund R, Vingsbo O, Vincent L, Guiraldenq P. Butterflies in fatigued ball-bearings – formation mechanisms and structure. Scand J Metall 1982;11:23–32.
[54] Liu W. The failure analysis of the repeat gear tooth breakage in a 40 Mw steam turbine load gearbox and the butterfly in the carburized case. Eng Fail Anal 2014;46:9–17.
[55] Grabulov A, Ziese U, Zandbergen HW. TEM/SEM investigation of microstructural changes within the white etching area under rolling contact fatigue and 3-D crack reconstruction by focused ion beam. Scripta Mater 2007;57:635–8.
[56] Uyama H, Yamada H, Hidaka H, Mitamura N. The effects of hydrogen on microstructural change and surface originated flaking in rolling contact fatigue. Tribol Online 2011;6:123–32.
[57] Buchwarld J, Heckel RW. An analysis of microstructural changes in 52100 steel bearings during cyclic stressing. Trans ASM 1968;61:750–6.
[58] Hiraoka K, Nagao M, Isomoto T. Study on flaking process in bearings by white etching area generation. In: Beswick JM, editor. Bearing Steel Technology-Advances and State of the Art in Bearing Steel Quality Assurance: 7th Volume, vol. 1465. W Conshohocken: American Society Testing and Materials; 2007. p. 234–40.
[59] Holweger W, Walther F, Loos J, Wolf M, Schreiber J, Dreher W, et al. Non-destructive subsurface damage monitoring in bearings failure mode using fractal dimension analysis. Ind Lubr Tribol 2012;64:132–7.
[60] Li YJ, Herbig M, Goto S, Raabe D. Formation of nanosized grain structure in martensitic 100cr6 bearing steels upon rolling contact loading studied by atom probe tomography. Mater Sci Technol 2016:1–6.
[61] Furuhara T, Kawata H, Morito S, Maki T. Crystallography of upper bainite in Fe–Ni–C alloys. Mater Sci Eng: A 2006;431:228–36.
[62] Kitahara H, Ueji R, Ueda M, Tsuji N, Minamino Y. Crystallographic analysis of plate martensite in Fe–28.5 At.% Ni by Fe-SEM/Ebsd. Mater Charact 2005;54:378–86.
[63] Greninger AB, Troiano AR. Orientation habit of martensite. Nature 1938;141:38.
[64] He Y. Grain-scale characterization of FCC/BCC correspondence relations and variant selection. Montreal, Canada: Department of Mining, Metals and Material Engineering, McGill University; 2005.
[65] Swahn H, Becker P, Vingsbo O. Electron-microscope studies of carbide decay during contact fatigue in ball bearings. Metal Sci 1976;10:35–9.
[66] Swahn H, Becker PC, Vingsbo O. Martensite decay during rolling-contact fatigue in ball-bearings. Metall Trans Phys Metall Mater Sci 1976;7:1099–110.
[67] Osterlund R, Vingsbo O. Phase-changes in fatigued ball-bearings. Metall Trans Phys Metall Mater Sci 1980;11:701–7.
[68] Evans MH, Wang L, Wood RJK. Formation mechanisms of white etching cracks and white etching area under rolling contact fatigue. Proc Inst Mech Eng Part J-J Eng Tribol 2014;228:1047–62.